Research Article

Nano Biomed Eng

Improving the Antibacterial Properties of SnO_2/Mn_3O_4 Hybrid Thin Film Synthesized by Spray Pyrolysis Method

Sabah Hassan Jumaah[1], Muayad Raheem Hussein[2], Nadir Fadhil Habubi[3], Sami Salman Chiad[1], Khalid Haneen Abass[4]

[1]Department of Physics, College of Education, Mustansiriyah University, Baghdad, Iraq
[2]General Directorate of Education in Thi-Qar, Ministry of Education, Rifai, Iraq
[3]Department of Radiation and Sonar Technologies, Alnukhba University College, Baghdad, Iraq
[4]Department of Physics, College of Education for Pure Sciences, University of Babylon, Babylon, Iraq

Corresponding author. E-mail: pure.khalid.haneen@uobabylon.edu.iq

Received: May 12, 2022; **Revised:** Oct. 08, 2022; **Accepted:** Nov. 02, 2022 **Published:** Nov. 30, 2022

Citation: S.H. Jumaah, M.R. Hussein, N.F. Habubi, et al. Improving the antibacterial properties of SnO_2/Mn_3O_4 hybrid thin film synthesized by spray pyrolysis method. *Nano Biomedicine and Engineering*, 2022, 14(3): 280–288.

DOI: 10.5101/nbe.v14i3.p280–288

Abstract

The current study used the spray pyrolysis method to prepare tin oxide, manganese oxide, and SnO_2/Mn_3O_4 hybrid bilayer thin films. The primary solutions for the deposition process were produced utilizing the sol-gel method. X-ray diffraction, energy-dispersive X-ray spectroscopy, field emission scanning electron microscopy (FESEM), Fourier transform infrared (FTIR) spectroscopy, and photoluminescence spectroscopy were used to analyze the grown films. XRD spectrum of SnO_2, Mn_3O_4, and SnO_2/Mn_3O_4 hybrid bilayer thin film shows that SnO_2 thin film has a polycrystalline structure with a tetragonal cassiterite phase, Mn_3O_4 thin film shows a lower crystallinity degree due to the powdery nature of its surface, and XRD pattern of SnO_2/Mn_3O_4 hybrid thin film has a polycrystalline structure. From the FESEM, the surface morphology of SnO_2 thin film is crack-free and regular with incessant grain distribution. FESEM micrographs of the synthesized Mn_3O_4 thin film and the perfectly spherical grains of Mn_3O_4 are uniform and entirely separate, with an average size of less than 50 nm. FESSEM micrographs of SnO_2/Mn_3O_4 hybrid thin film exhibit an uneven and porous polycrystalline structure with polyhedral granulation. The film's antibacterial properties were evaluated for standard gram-negative bacteria (GNB) and gram-positive bacteria (GPB), namely *Staphylococcus aureus* and *Escherichia coli*. According to the results, the hybrid bilayers have demonstrated better antibacterial properties than tin oxide and manganese oxide monolayers. These findings ascertain the role the hybrid thin film nanocomposites play in the biomedical field's potential applications.

Keywords: SnO_2; Mn_3O_4; SnO_2/Mn_3O_4 hybrid; Spray pyrolysis; Antibacterial properties

Introduction

The disinfection of water, sewage, and various surfaces is essential in domestic consumption and different industries. It is obvious since, for instance, different surfaces contain large amounts of microorganisms, which renders the need to use antimicrobial agents that negatively impact the environment of particular importance. Conventional methods such as ultraviolet light, ozone, and chlorine dioxide are effective against most pathogens [1–4]. However, these chemical disinfectants can react with wide variety of compounds in water or air, many of which are deemed carcinogenic, in addition to the fact that the synthesis methods are usually costly, thus, are not economical on a large scale [5–7].

The photocatalyst materials are the most straightforward and inexpensive methods of dealing with microorganisms [8]. Antimicrobial minerals are used in various forms, such as powder. The problem with using the powder is that the particles may agglomerate and disrupt the photocatalytic performance. In addition, powdery materials are difficult to separate and recover. For these reasons, using motionless photocatalysts such as thin films has been recently considered by researchers [9–11].

Matsunaga et al. first reported on titanium dioxide's antibacterial properties in 1985 [12]. After that, researchers considered semiconductor materials with significant band gaps, such as zinc oxide, silicon oxide, and tin oxide, where intensive work was devoted to investigating the antibacterial properties of these materials [13–18]. Tin oxide- and manganese oxide-based nanocomposites were potential materials for that researchers have intensively examined their antibacterial activity. For instance, Talebian et al. studied the antibacterial properties of ZnO/SnO_2 nanocomposite thin film on *E. coli*. Their results showed that the nanocomposite's antibacterial activity was better than that of the thin film of tin oxide and zinc oxide alone [19]. Additionally, Henry et al. revealed that the sol-gel spin coating method of tin oxide thin film has good antibacterial action against *Bacillus* and *E. coli*. [20]. In another work, Belkhedkar and Ubale found that the antibacterial activity of manganese oxide thin film was significantly enhanced by increasing its film thickness [21]. In their later research, Belkhedkar and Ubale investigated the impact of adding iron impurities on the antibacterial properties of Mn_3O_4 thin film. According to the study results, manganese oxide had a very high antibacterial activity, further increasing iron impurities [22]. Omar et al. examined the antibacterial and antifungal activities of ZnO-SnO_2 nanocomposite, which was grown by the sol-gel method, against different types of bacteria and fungi. Their findings showed greater effectiveness of ZnO-SnO_2 nanocomposite with 7 mg/cm^3 concentration against the gram-positive bacteria and fungi with inhibition ability of 80% [23].

In another work, Phukan et al. demonstrated a reasonable inhibition rate of successfully synthesized SnO_2 nanoparticles supported with montmorillonite clay against GPB and GNP strains [24]. Most recently, Sathishkumar and Geethalakshmi managed to promote the antibacterial activity against *P. aeruginosa* and *S. aureus* microorganisms using SnO_2 nanoparticles doped with 9% (mass fraction) of Cu content, which was produced via a simple microwave-assisted method.

Although manganese oxide was reported to demonstrate excellent antibacterial properties, in general, very few articles have examined its antibacterial activity. Furthermore, no research has been conducted to explore the antibacterial properties of bilayer thin film composed of tin oxide/manganese oxide. Thus, this research was meant to investigate the antibacterial properties of tin oxide/manganese oxide bilayer thin film nanocomposite and compare the obtained results with the monolayer of these structures. As far as the author knows, this is the first trial using a bilayer of SnO_2/Mn_3O_4 to enhance the antibacterial properties.

Materials and Methods

Materials

Merck Sigma Aldrich supplied all the necessary precursors and chemicals used in this research. The standard GNB of Escherichia coli DH5 alpha (ATCC 25922) (1399PTCC) and gram-positive bacterium of Staphylococcus aureus were purchased from Iran's Scientific Industrial Research Centre.

Monolayer and bilayer thin films preparation

Initial solutions were prepared using tin chloride ($SnCl_2 \cdot 5H_2O$) and manganese acetate ($C_4H_6MnO_4$) precursors via the sol-gel method, as reported in previous research works [25, 26]. Tin oxide solution was prepared by mixing tin chloride (0.10 mol/L) and ethanol with appropriate molar ratios of 1:1.2 under vigorous stirring at ambient temperature. A white solution was obtained, which was discarded for 24 h until the solution color changed to clear yellow. Manganese acetate (0.10 mol/L), citric acid, and propyl alcohol were mixed with appropriate molar ratios of 0.1:1:1 to prepare a manganese oxide solution, and the solution was stirred for 12 h. The pH of the solution was set to 9 using ammonium hydroxide. Subsequently, acetone and an ultrasonic bath were used to clean glass substrates and deposit the synthesized solutions, which was carried out using spray pyrolysis technique. The deposition parameters, such as substrate temperature, solution spray rate, and substrate-nozzle distance, were 500 °C, 3 mL/min, and 30 cm, respectively. The detailed procedures used to perform the experimental preparation of the monolayer and bilayer thin films are depicted in Fig. 1.

Characterization of monolayer and bilayer thin films

The properties of the prepared monolayer of SnO_2 and Mn_3O_4, as well as its hybrid bilayer thin film of SnO_2/Mn_3O_4, were examined using different characterization tools. The structural properties were analyzed using XRD (Model D8 Advance Bruker YT diffractometer) via CuKα radiation of λ = 1.5418 Å in the 2θ range of 5°—80°. FESEM (Model MIRA3 TESCAN-XMU) equipped with EDX spectrophotometer was employed to examine the morphology of the surface and elemental chemical composition of the gained thin films. FTIR (Model Nicolet AVATAR 370) was used in the area of 400—4000 cm^{-1} to confirm the successful synthesis of the monolayer and hybrid bilayer thin films by examining the chemical bonds' vibrational modes in each sample. The photoluminescence properties were investigated employing the PL device (Model Perkin Elmer LS 45) in the area of 400—800 nm, and the antibacterial properties of the synthesized monolayer and hybrid bilayer thin films against standard GNB and GPB were evaluated.

Results and Discussion

XRD analysis

The XRD spectrum of SnO_2 thin film is shown in Fig. 2(a) and is marked with black. Diffraction peaks with plane indices of (110), (101), (111), (211), (220), (221), and (112) referred to the formation of SnO_2 crystalline structure with a tetragonal cassiterite phase (JCPDS Card No. 41-1445). The lattice parameters of a = 4.71 Å and c = 3.19 Å were obtained, which perfectly accord with the bulk values published by other researchers [27–29].

XRD spectrum of Mn_3O_4 thin film deposited using the spray pyrolysis method is shown in Fig. 2(b). The Mn_3O_4 thin film shows a lower crystallinity degree because of its powdery surface. Poor crystallization of the structure might be due to the impact of saturation reaction and atomic species re-evaporation throughout spraying from the nozzle to the substrate [30]. The diffraction peaks related to plane indices of (101), (112), (103), (211), (004), (220), and with (103) predominant orientation confirm the formation of Mn_3O_4 tetragonal phase with I41/amd spatial group as compared with the standard value of JCPDS-24-0734.

The XRD pattern of SnO_2/Mn_3O_4 hybrid thin film

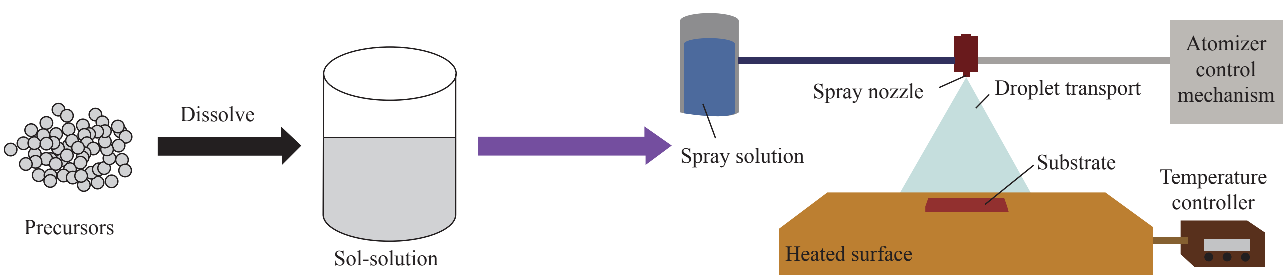

Fig. 1 Experimental preparation procedures of the monolayer and bilayer thin films

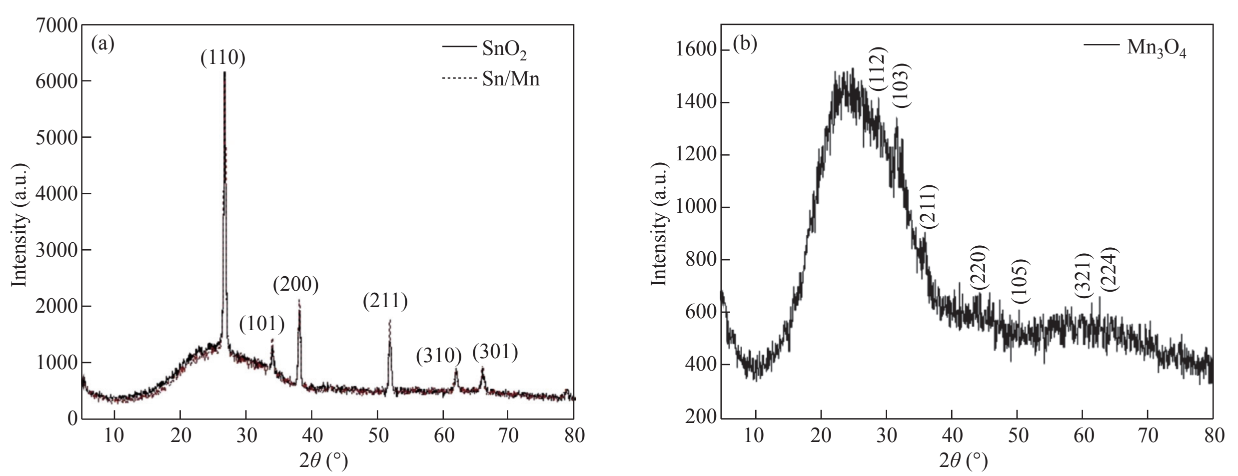

Fig. 2 XRD spectrum of **(a)** SnO_2 thin film (black color) and SnO_2/Mn_3O_4 hybrid bilayer (red dotted line), **(b)** Mn_3O_4 thin film synthesized by spray pyrolysis method

nanocomposite synthesized by spray pyrolysis method, shown in Fig. 2(a) with the red dotted line, suggests that it has a polycrystalline structure. X'Pert software was used to validate the existence of the two phases of SnO_2 and Mn_3O_4, which agrees with the standard values of 01-077-0447 for SnO_2 and 01-089-4837 for Mn_3O_4. Given that the intensity of the peaks related to manganese oxide is much lower than that of tin oxide, and SnO_2 layer is synthesized on the Mn_3O_4 layer, the presence of these peaks related to Mn_3O_4 in the hybrid thin film nanocomposite is inconspicuous.

The crystal size was calculated based on the most intense peak for all thin film samples using Scherrer's formula that is given by

$$d = k\lambda/(\beta\cos\theta) \tag{1}$$

where d is the crystal's grain size, k = 0.9, λ = 0.154 nm is the X-ray wavelength of CuKα source, β is FWHM of the most intense peak, and θ is the Bragg's diffraction angle [31–34]. The mean crystal's grain sizes of SnO_2, Mn_3O_4, and SnO_2/Mn_3O_4 thin films calculated based on their most intense peak are shown in Table 1.

SEM and EDX analysis

The morphological behavior was investigated using FESEM, as illustrated in Fig. 3. It is seen that the SnO_2 thin film surface morphology, as depicted in Fig. 3(a), is crack-free and uniform with a continuous grain distribution. Large polyhedral grains in this micrograph indicate the formation of tightly packed-shaped crystals. The structure of the formed grains is similar to that reported by other researchers [35, 36]. FESEM micrographs of the synthesized Mn_3O_4 thin film are shown in Fig. 3(b). According to the images, the perfectly spherical grains of Mn_3O_4 are uniform and entirely separate, with an average size of less than 50 nm. Figure 3(c) shows the FESSM micrographs of SnO_2/Mn_3O_4 hybrid thin film nanocomposite. The bilayer thin film sample exhibits an uneven and porous polycrystalline structure with polyhedral granulation. The elemental composition of SnO_2/Mn_3O_4 hybrid thin film nanocomposite was analyzed using energy-dispersive spectroscopy, as shown in Fig. 4. The presence of Sn and Mn elements confirms the formation of tin oxide/manganese oxide hybrid bilayer.

FTIR analysis

FTIR measurements performed for monolayer and bilayer in the area of 400—4000 cm^{-1} are illustrated in Fig. 5. As manifested in Fig. 5(a), the FTIR spectrum of SnO_2 thin film shows a strong band noticed at 1000 cm^{-1}, which is specified to the vibration of Sn—OH, while the bands seen at 760 and 500 cm^{-1} are related to Sn—O—Sn and Sn—O bending vibrations, respectively [37-39]. The observed bands in the 3000—3600 cm^{-1} range are related to the stretching vibrations of hydroxyl groups [40]. Figure 5(b) demonstrates the spectrum of Mn_3O_4 thin film. It is apparent that the spectrum exhibits three distinct bands at 609, 513, and 413 cm^{-1}, which are ascribed to stretching vibrations of Mn—O and Mn—O—Mn, respectively [41, 42].

Table 1 Crystal's grain size of SnO_2, Mn_3O_4 and SnO_2/Mn_3O_4 thin films

SnO_2		Mn_3O_4		SnO_2/Mn_3O_4	
2θ(°)	D (nm)	2θ(°)	D (nm)	2θ(°)	D (nm)
26.627	25.83	29.1749	14.03	26.634	25.44

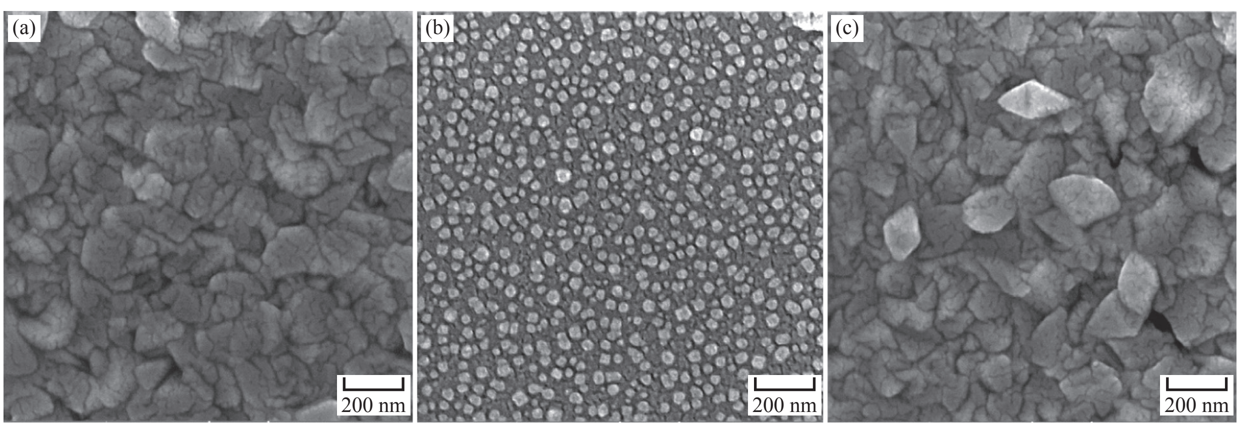

Fig. 3 FESEM Micrographs of **(a)** SnO_2 thin film, **(b)** Mn_3O_4 thin film and **(c)** SnO_2/Mn_3O_4 hybrid bilayer synthesized by spray pyrolysis method

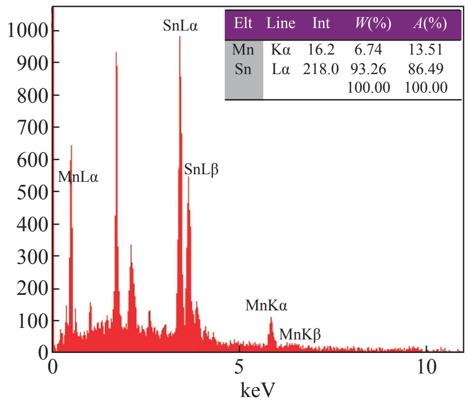

Fig. 4 EDS of SnO_2/Mn_3O_4 hybrid thin film

Finally, the formation of SnO_2/Mn_3O_4 hybrid thin film nanocomposite is made evident by the spectrum shown in Fig. 5(c), where all vibrations at the bands designated for the monolayers of SnO_2 and Mn_3O_4 are observed.

Optical properties

The obtained photoluminescence spectra of monolayer and bilayer thin films in the area of 400—800 nm are demonstrated in Fig. 6. When excited at 450 nm, one visible peak appeared at 650 nm. The photoluminescence spectrum of SnO_2 thin film shown in Fig. 6(a) exhibits a prominent peak at 650 nm. The main peak recorded at about 650 nm is ascribed to a defect-related luminescence, possibly because of the oxygen vacancies and unoccupied electron states in the dangling bonds of the SnO_2 crystal's surface [43].

Figure 6(b) shows the photoluminescence spectrum of Mn_3O_4 thin film with an excitation wavelength of 275 nm. As can be seen, four emission peaks at 399, 416, 449, and 498 nm were attained. The emission bands set at 399 nm and 416 nm correspond to the recombination and emission of free excitons through an exciton-exciton collision process near band edges. A prominent blue emission at 449 nm and a green emission monitored at 498 nm can be assigned to the radial recombination of the photo-generated hole with an electron resulting in singly ionized oxygen vacancy-related defects [44].

Finally, Fig. 6(c) shows the emission spectrum of SnO_2/Mn_3O_4 bilayer hybrid thin film nanocomposite. The PL spectra of this sample show broad UV and low intense visible peaks at about 420 and 750 nm, respectively, when excited at 368 nm. The emission spectrum shows a strong band at 420 nm. From another perspective, it is noticed that the deposition of

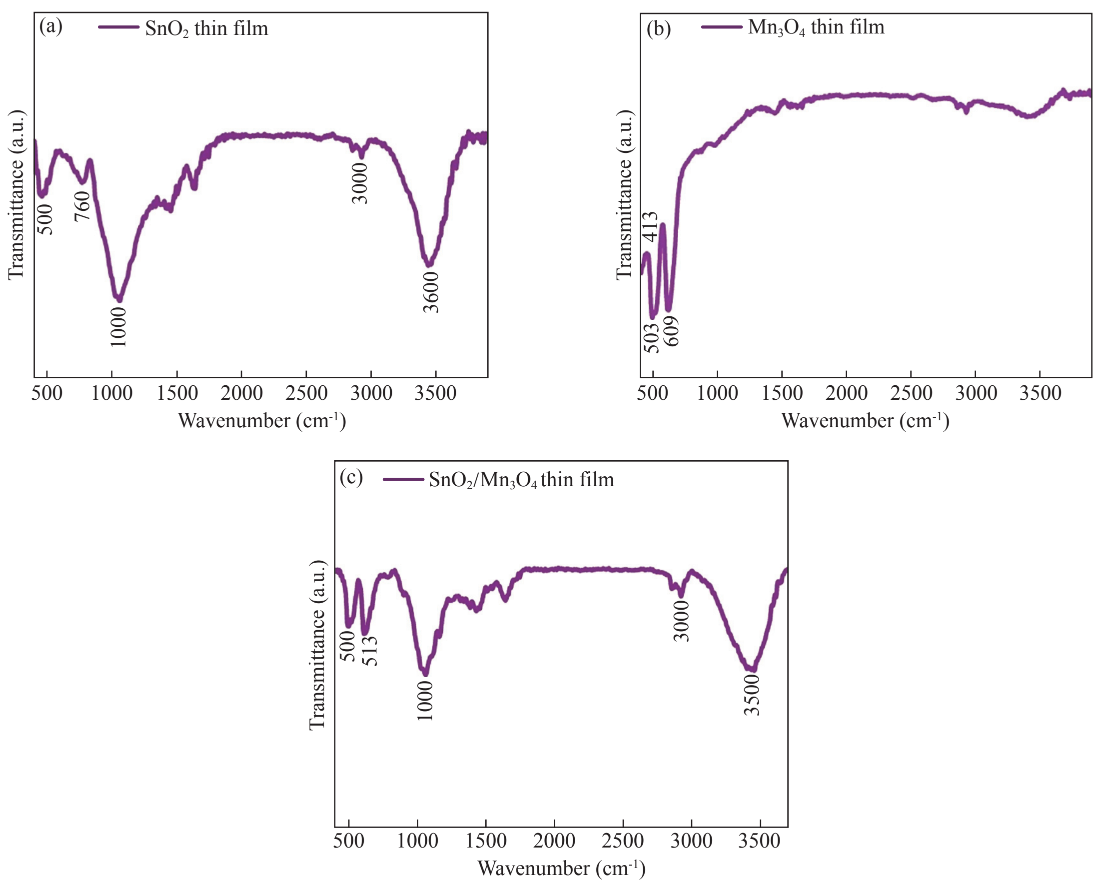

Fig. 5 FTIR spectra of the thin films of **(a)** Mn_3O_4, **(b)** SnO_2 and **(c)** SnO_2/Mn_3O_4

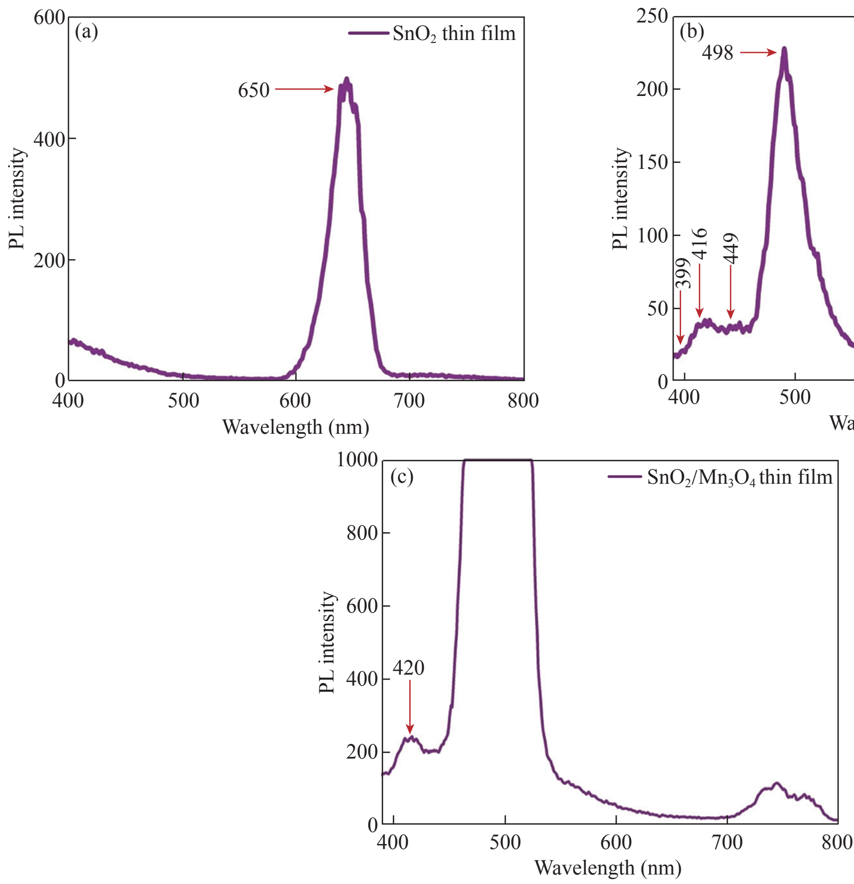

Fig. 6 Photoluminescence spectra of the thin films of **(a)** Mn_3O_4, **(b)** SnO_2, and **(c)** SnO_2/Mn_3O_4

SnO_2 film on Mn_3O_4 film reduced the intensity of the photoluminescence light produced. For pure SnO_2 thin film, the emission resulting from the electron transfer is mediated by the level of a defect in the band gap, such as tin interstitial and oxygen vacancy. Therefore, defects in the luminescence process played a significant role after depositing SnO_2 on Mn_3O_4 film.

Antibacterial properties

The antibacterial properties of SnO_2, Mn_3O_4, and SnO_2/Mn_3O_4 heterojunction were investigated. The experimental results obtained for *Staphylococcus aureus* and *Escherichia coli* bacteria, when cultured on an empty glass substrate and the surfaces of these thin films for 24 h, are manifested in Figs. 7 and 8.

Notably, the diffusion of metal ions is crucial in determining antibacterial activity [45]. Various mechanisms behind bacterial growth inhibition because of the metal oxide nanostructures were reported, including nanostructures decomposition, reactive oxygen species formation, electrostatic interaction of nanostructures having cell walls, and their photocatalytic optical activity [46, 47]. As evident in Fig. 7, the antibacterial activity of SnO_2 thin film against *Staphylococcus aureus* exhibited inhibition

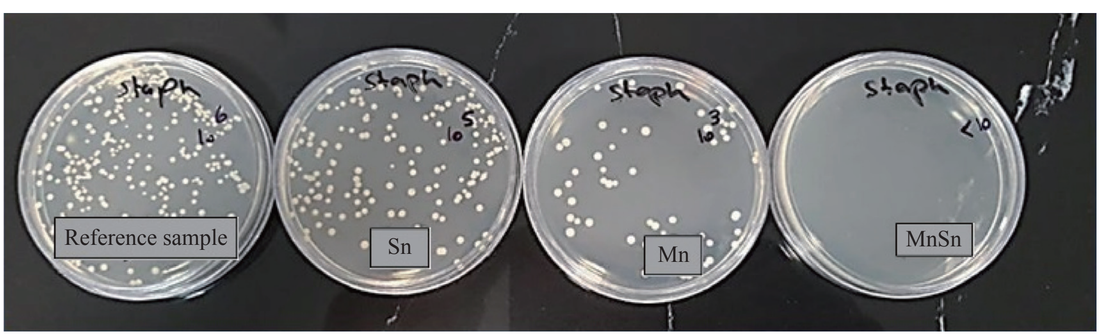

Fig. 7 Inhibition percentage of *Staphylococcus aureus* growth on SnO_2, Mn_3O_4, and SnO_2/Mn_3O_4 heterojunction thin films, Sn > 80%, Mn > 90%, MnSn > 99%

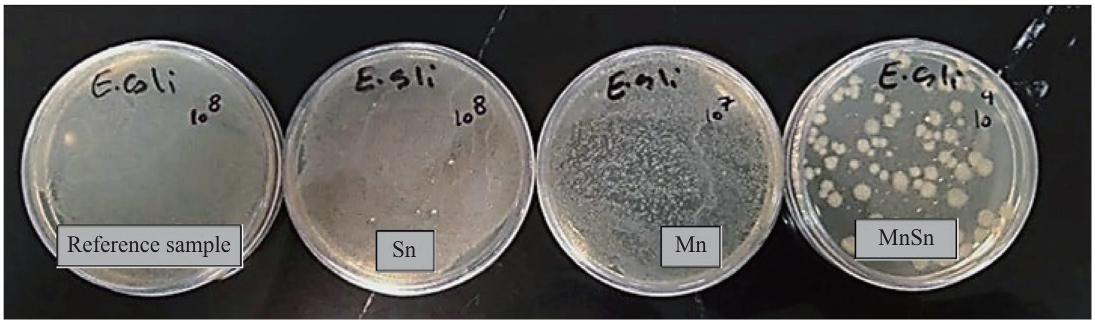

Fig. 8 Inhibition percentage of *Escherichia coli* growth on SnO_2, Mn_3O_4, and SnO_2/Mn_3O_4 heterojunction thin films, Sn >70%, Mn > 80%, MnSn > 99%

of bacterial growth of about 80%. On the other hand, the antibacterial efficacy against *Staphylococcus aureus* cultured on Mn_3O_4 thin film showed inhibition of bacterial growth of more than 90%. These results are believed to be related to the increase in manganese and hydroxyl ions released from the surface, which destroyed the surface microorganisms. More interestingly, it was found that the percentage of bacterial growth inhibition of the SnO_2/Mn_3O_4 heterojunction thin film was much better than that of the previous two films, which was above 99%. Various factors affect the antibacterial activity, including the concentration of nanoparticles used. Many studies show that increasing the concentration of nanoparticles increases their antibacterial activity [48–51]. In the bilayer sample, the concentration of nanoparticles is higher than in the monolayer samples, so the bilayer sample shows much higher antibacterial activity than the monolayer samples.

Similarly, as observed in Fig. 8, SnO_2, Mn_3O_4, and SnO_2/Mn_3O_4 heterojunction thin films, compared with the control sample, have also inhibited the *Escherichia coli* bacterial growth of more than 70%, 80%, and 99%, respectively. It is seen that the deposition of SnO_2 and Mn_3O_4 on each other and the successful creation of the heterojunction had a significant impact on inhibiting the growth of both GPB and GNB. The reason for more resistance of *Escherichia coli* to *Staphylococcus aureus* is the difference between the membrane structure of GNB and GPB, and the difference in the thickness of their peptidoglycans. GPB, such as *Staphylococcus aureus*, has multilayered and thick peptidoglycans. Still, GNB, such as *Escherichia coli*, has thinner peptidoglycans, but their outer membrane contains lipopolysaccharide and low permeability to antibiotic and antibiotic agents. Therefore, the efficiency of the synthesized thin films against *Staphylococcus aureus* is higher than that of *Escherichia coli*.

Conclusion

In this research, primary solutions of tin oxide and manganese oxide were prepared using the sol-gel method. Then, tin oxide, manganese oxide thin films, and SnO_2/Mn_3O_4 hybrid bilayers thin film were deposited by the spray pyrolysis method at a temperature of about 500 °C. The XRD spectrum and EDX results confirmed the desired structures formed without impurities. According to FESEM images, the grain size in all samples was on a nanometer scale. FTIR measurements in the 400—1000 cm^{-1} were performed for all the studied films, and the existing peaks for the produced thin films were confirmed. Furthermore, the photoluminescence spectroscopy of the films showed that the deposition of SnO_2 film on Mn_3O_4 film had reduced the intensity of photoluminescence light of SnO_2. Measurement of the monolayer and bilayer films' antibacterial properties against the standard gram-negative and gram-positive bacteria of *Escherichia coli* and *Staphylococcus aureus*, respectively, showed that the hybrid bilayer had demonstrated better antibacterial properties as compared with that of tin oxide and manganese oxide monolayers.

Reference

[1] T. Jäger, J. Alexander, S. Kirchen, et al. Live-dead discrimination analysis, qPCR assessment for opportunistic pathogens, and population analysis at ozone wastewater treatment plants. *Environmental Pollution*, 2018, 232: 571–579. http://dx.doi.org/10.1016/j.envpol.2017.09.089

[2] K. Song, M. Mohseni, F. Taghipour. Application of ultraviolet light-emitting diodes (UV-LEDs) for water disinfection: A review. *Water Research*, 2016, 94: 341–349. http://dx.doi.org/10.1016/j.watres.2016.03.003

[3] M. Remondino, L. Valdenassi. Different uses of ozone: Environmental and corporate sustainability. literature review and case study. *Sustainability*, 2018, 10(12): 4783. https://doi.org/10.3390/su10124783

[4] B. Casini, B. Tuvo, M.L. Cristina, et al. Evaluation of an ultraviolet C (UVC) light-emitting device for disinfection of high touch surfaces in hospital critical areas. *Journal of Environmental Research and Public Health*, 2019, 16(19): 3572. https://doi.org/10.3390/ijerph16193572

[5] Z.J. Zhou, S. Zuber, F. Cantergiani, et al. Inactivation of foodborne pathogens and their surrogates on fresh and frozen strawberries using gaseous ozone. *Frontiers in Sustainable Food Systems*, 2018, 2: 51. https://doi.org/10.3389/fsufs.2018.00051

[6] R.X. Chang, P. Pandey, Y.M. Li, et al. Assessment of gaseous ozone treatment on *Salmonella* Typhimurium and *Escherichia coli* O157: H7 reductions in poultry litter. *Waste Management*, 2020, 117: 42–47. http://dx.doi.org/10.1016/j.wasman.2020.07.039

[7] V.M. Gómez-López, A. Rajkovic, P. Ragaert, et al. Chlorine dioxide for minimally processed produce preservation: A review. *Trends in Food Science & Technology*, 2009, 20: 17–26. http://dx.doi.org/10.1016/j.tifs.2008.09.005

[8] I. Sondi, B. Salopek-Sondi. Silver nanoparticles as antimicrobial agent: A case study on *E. coli* as a model for Gram-negative bacteria. *Journal of Colloid and Interface Science*, 2004, 275: 177–182. http://dx.doi.org/10.1016/j.jcis.2004.02.012

[9] H.L. Liu, T.C.K. Yang. Photocatalytic inactivation of *Escherichia coli* and *Lactobacillus helveticus* by ZnO and TiO_2 activated with ultraviolet light. *Process Biochemistry*, 2003, 39: 475–481. http://dx.doi.org/10.1016/S0032-9592(03)00084-0

[10] K.H. Tam, A.B. Djurišić, C.M.N. Chan, et al. Antibacterial activity of ZnO nanorods prepared by a hydrothermal method. *Thin Solid Films*, 2008, 516: 6167–6174. http://dx.doi.org/10.1016/j.tsf.2007.11.081

[11] C.L. Ren, B.F. Yang, M. Wu, et al. Synthesis of Ag/ZnO nanorods array with enhanced photocatalytic performance. *Journal of Hazardous Materials*, 2010, 182: 123–129. http://dx.doi.org/10.1016/j.jhazmat.2010.05.141

[12] T. Matsunaga, R. Tomoda, T. Nakajima, et al. Photoelectrochemical sterilization of microbial cells by semiconductor powders. *FEMS Microbiology Letters*, 1985, 29: 211–214.

[13] Q. Guo, C.Y. Zhou, Z.B. Ma, et al. Fundamentals of TiO_2 photocatalysis: Concepts, mechanisms, and challenges. *Advanced Materials*, 2019, 31: e1901997. https://doi.org/10.1002/adma.201901997

[14] A. Yiannikouris, J. François, L. Poughon, et al. Alkali extraction of beta-d-glucans from *Saccharomyces cerevisiae* cell wall and study of their adsorptive properties toward Zearalenone. *Journal of Agricultural and Food Chemistry*, 2004, 52: 3666–3673. https://doi.org/10.1021/jf035127x

[15] L. Motevalizadeh, B.G. Shohany, M.E. Abrishami. Effects of Mn doping on electrical properties of ZnO thin films. *Modern Physics Letters B*, 2016, 30: 1650024. https://doi.org/10.1142/s021798491650024x

[16] R. Abrashev, P. Dolashka, R. Christova, et al. Role of antioxidant enzymes in survival of conidiospores of *Aspergillus niger* 26 under conditions of temperature stress. *Journal of Applied Microbiology*, 2005, 99: 902–909. https://doi.org/10.1111/j.1365-2672.2005.02669.x

[17] A. Jalaukan, S.M. Aldowaib, A.S. Hamed, et al. Photocatalytic activity, antibacterial effect, and self cleaning properties of TiO_2/GO thin films. *Iranian Journal of Materials Science and Engineering*, 2019, 16(4): 53–62. http://khabgah.iust.ac.ir/ijmse/article-1-1432-en.pdf

[18] B.S. Xu, M. Niu, L.Q. Wei, et al. The structural analysis of biomacromolecule wool fiber with Ag-loading SiO_2 nano-antibacterial agent by UV radiation. *Journal of Photochemistry and Photobiology A*: *Chemistry*, 2007, 188: 98–105. http://dx.doi.org/10.1016/j.jphotochem.2006.11.025

[19] N. Talebian, M.R. Nilforoushan, E.B. Zargar. Enhanced antibacterial performance of hybrid semiconductor nanomaterials: ZnO/SnO_2 nanocomposite thin films. *Applied Surface Science*, 2011, 258: 547–555. http://dx.doi.org/10.1016/j.apsusc.2011.08.070

[20] J. Henry, K. Mohanraj, G. Sivakumar, et al. Electrochemical and fluorescence properties of SnO_2 thin films and its antibacterial activity. *Spectrochimica Acta Part A*: *Molecular and Biomolecular Spectroscopy*, 2015, 143: 172–178. http://dx.doi.org/10.1016/j.saa.2015.02.034

[21] M.R. Belkhedkar, A.U. Ubale. Physical properties of nanostructured Mn_3O_4 thin films synthesized by SILAR method at room temperature for antibacterial application. *Journal of Molecular Structure*, 2014, 1068: 94–100. http://dx.doi.org/10.1016/j.molstruc.2014.03.050

[22] M.R. Belkhedkar, A.U. Ubale. Physical properties of Fe doped Mn_3O_4 thin films synthesized by SILAR method and their antibacterial performance against *E. coli*. *Journal of Saudi Chemical Society*, 2016, 20: 553–560. http://dx.doi.org/10.1016/j.jscs.2014.11.004

[23] K.A. Omar, B.I. Meena, S. Muhammed. Study on the activity of ZnO-SnO_2 nanocomposite against bacteria and fungi. *Physicochemical Problems of Mineral Processing*, 2016, 52: 754–766. http://dx.doi.org/10.5277/PPMP160219

[24] A. Phukan, R.P. Bhattacharjee, D.K. Dutta. Stabilization of SnO_2 nanoparticles into the nanopores of modified Montmorillonite and their antibacterial activity. *Advanced Powder Technology*, 2017, 28: 139–145. http://dx.doi.org/10.1016/j.apt.2016.09.005

[25] H. Baqiah, N.B. Ibrahim, S.A. Halim, et al. The role of cobalt doping on magnetic and optical properties of indium oxide nanostructured thin film prepared by Sol-gel method. *Materials Research Bulletin*, 2015, 63: 147–154. http://dx.doi.org/10.1016/j.materresbull.2014.12.006

[26] H. Baqiah, N.B. Ibrahim, S.A. Halim, et al. Conducting mechanisms and magnetic behaviours of Fe-doped In_2O_3 nanocrystalline films. *Results in Physics*, 2017, 7: 1115–1121. http://dx.doi.org/10.1016/j.rinp.2017.03.004

[27] L.P. Singh, M.N. Luwang, S.K. Srivastava. Luminescence and photocatalytic studies of Sm^{3+} ion doped SnO_2 nanoparticles. *New Journal of Chemistry*, 2014, 38: 115-121. http://dx.doi.org/10.1039/C3NJ00759F

[28] X. Zhang, Y. Yang, S. Ding, et al. Construction of high-quality SnO_2@MoS_2 nanohybrids for promising photoelectrocatalytic applications. *Inorganic Chemistry*, 2017, 56: 3386–3393. https://doi.org/10.1021/acs.inorgchem.6b02914

[29] R. Kalai, A. Otmani, L. Bechiri, et al. Effect of the substrate temperature on the properties of SnO_2 thin films prepared by ultrasonic spray for solar cells applications. *Journal of Nano Research*, 2019, 59: 126–136. https://doi.org/10.4028/www.scientific.net/jnanor.59.126

[30] A. Moses Ezhil Raj, S.G. Victoria, V.B. Jothy, et al. XRD and XPS characterization of mixed valence Mn_3O_4 hausmannite thin films prepared by chemical spray pyrolysis technique. *Applied Surface Science*, 2010, 256: 2920–2926. http://dx.doi.org/10.1016/j.apsusc.2009.11.051

[31] M.H. Flaifel, S.H. Ahmad, M.H. Abdullah, et al. NiZn ferrite filled thermoplastic natural rubber nanocomposites: Effect of low temperature on their magnetic behaviour. *Cryogenics*, 2012, 52: 523–529. http://dx.doi.org/10.1016/j.cryogenics.2012.06.009

[32] N.M. Al-Hada, E.B. Saion, A.H. Shaari, et al. Synthesis, structural and morphological properties of cadmium oxide nanoparticles prepared by thermal treatment method. *Advanced Materials Research*, 2015, 1107: 291–294.

https://doi.org/10.4028/www.scientific.net/amr.1107.291
[33] H. Kamari, N. Al-Hada, E. Saion, et al. Calcined solution-based PVP influence on ZnO semiconductor nanoparticle properties. *Crystals*, 2017, 7: 2. https://doi.org/10.3390/cryst7020002
[34] N.M. Al-Hada, H.M. Kamari, M.A. Saleh, et al. Morphological, structural and optical behaviour of PVA capped binary $(NiO)_{0.5}$ $(Cr_2O_3)_{0.5}$ nanoparticles produced via single step based thermal technique. *Results in Physics*, 2020, 17: 103059. http://dx.doi.org/10.1016/j.rinp.2020.103059
[35] A.R. Babar, S.S. Shinde, A.V. Moholkar, et al. Physical properties of sprayed antimony doped tin oxide thin films: The role of thickness. *Journal of Semiconductors*, 2011, 32: 053001. https://doi.org/10.1088/1674–4926/32/5/053001
[36] N.M. Al-Hada, A.M. Al-Ghaili, H. Kasim, et al. The effect of PVP concentration on particle size, morphological and optical properties of cassiterite nanoparticles. *IEEE Access*, 2020, 8: 93444–93454. http://dx.doi.org/10.1109/ACCESS.2020.2993689
[37] S.N. Pusawale, P.R. Deshmukh, C.D. Lokhande. Chemical synthesis of nanocrystalline SnO_2 thin films for supercapacitor application. *Applied Surface Science*, 2011, 257: 9498–9502. http://dx.doi.org/10.1016/j.apsusc.2011.06.043
[38] D. Vasanth Raj, N. Ponpandian, D. Mangalaraj, et al. Electrochemical behavior of nanostructured SnO_2 thin films in aqueous electrolyte solutions. *Materials Science in Semiconductor Processing*, 2014, 26: 55–61. http://dx.doi.org/10.1016/j.mssp.2014.04.003
[39] A. Martyla, M. Kopczyk, P. Marciniak, et al. One-pot method of synthesis of Pt/SnO_2 system and its electrocatalytic activity. *Chemistry Central Journal*, 2014, 8: 49. http://dx.doi.org/10.1186/s13065-014-0049-0
[40] S. Chaisitsak. Nanocrystalline SnO_2: F thin films for liquid petroleum gas sensors. *Sensors*, 2011, 11: 7127–7140. https://doi.org/10.3390/s110707127
[41] H.M. Chen, J.H. He. Facile synthesis of monodisperse Manganese oxide nanostructures and their application in water treatment. *The Journal of Physical Chemistry C*, 2008, 112: 17540–17545. https://doi.org/10.1021/jp806160g
[42] C.C. Huang, N.H. Khu, C.S. Yeh. The characteristics of sub 10 nm Manganese oxide T_1 contrast agents of different nanostructured morphologies. *Biomaterials*, 2010, 31: 4073–4078. http://dx.doi.org/10.1016/j.biomaterials.2010.01.087
[43] F. Gu, shu fen Wang, meng kai Lü, et al. Photoluminescence properties of SnO_2 nanoparticles synthesized by Sol-gel method. *The Journal of Physical Chemistry B*, 2004, 108: 8119–8123. https://doi.org/10.1021/jp036741e
[44] A.M. Toufiq, F.P. Wang, Q.U.A. Javed, et al. Synthesis, characterization and photoluminescent properties of 3D nanostructures self-assembled with Mn_3O_4 nanoparticles. *Materials Express*, 2014, 4: 258–262. https://doi.org/10.1166/mex.2014.1167
[45] V.K. Vidhu, D. Philip. Biogenic synthesis of SnO_2 nanoparticles: Evaluation of antibacterial and antioxidant activities. *Spectrochimica Acta Part A*: *Molecular and Biomolecular Spectroscopy*, 2015, 134: 372–379. http://dx.doi.org/10.1016/j.saa.2014.06.131
[46] Z.P. Wang, Y.H. Lee, B. Wu, et al. Anti-microbial activities of aerosolized transition metal oxide nanoparticles. *Chemosphere*, 2010, 80: 525–529. http://dx.doi.org/10.1016/j.chemosphere.2010.04.047
[47] N.M. Al-Hada, H.M. Kamari, C.A.C. Abdullah, et al. Down-top nanofabrication of binary $(CdO)_x$ $(ZnO)_{1-x}$ nanoparticles and their antibacterial activity. *International Journal of Nanomedicine*, 2017, 12: 8309–8323. https://doi.org/10.2147/ijn.s150405
[48] S.M.H. AL-Jawad, S.H. Sabeeh, A.A. Taha, et al. Studying structural, morphological and optical properties of nanocrystalline ZnO: Ag films prepared by Sol-gel method for antimicrobial activity. *Journal of Sol-Gel Science and Technology*, 2018, 87: 362–371. http://dx.doi.org/10.1007/s10971-018-4724-9
[49] S.M. Al-Jawad, S.H. Sabeeh, A.A. Taha, et al. Synthesis and characterization of fe-zno thin films for antimicrobial activity. *Surface Review and Letters*, 2019, 26: 1850197. https://doi.org/10.1142/s0218625x18501974
[50] S.M.H. Al-Jawad, A.A. Taha, A.M. Redha, et al. Influence of nickel doping concentration on the characteristics of nanostructure cus prepared by hydrothermal method for antibacterial activity. *Surface Review and Letters*, 2021, 28: 2050031. https://doi.org/10.1142/s0218625x20500316
[51] Z.S. Shakir, S.M.H. AL-Jawad, D.S. Ahmed. Influence of cobalt doping concentration on ZnO/MWCNTs hybrid prepared by Sol-gel method for antibacterial activity. *Journal of Sol-Gel Science and Technology*, 2021, 100: 115–131. http://dx.doi.org/10.1007/s10971-021-05603-0